

DNS AND LES STUDIES ON TURBULENT HEAT TRANSFER PHENOMENA OF ROUND IMPINGING JET IN FINITE VESSEL

H. Hattori

Advanced Manufacturing Research Center, Nagoya Institute of Technology
Gokiso-cho, Showa-ku, Nagoya 466-8555, Japan
hattori@nitech.ac.jp

T. Mizukami, H. Baba, T. Houra and M. Tagawa

Department of Electrical and Mechanical Engineering, Nagoya Institute of Technology

INTRODUCTION

Technology of enhancement of heat transfer using turbulence is very important factor for increase of heat efficiency of thermal equipment. In such a technology, since the impingement jet gives higher heat transfer rate around the stagnation point, the impinging jet is widely used for the cooling of wall, etc. Heat transfer rate, however, rapidly decreases toward downstream region on the impingement wall, so it is difficult to effectively use the impinging jet for the enhancement of heat transfer in wide region. Thus, it is important to know the characteristics, structures, and statistical quantities of turbulent heat transfer phenomena of impinging jet for the enhancement of heat transfer rate using it. In the previous study (Hattori & Nagano, 2004), the plane impinging jet with short impingement distance has been investigated by direct numerical simulation (DNS), in which it is found the appearance of the second peak of local Nusselt number. So, to enhance heat transfer rate using the impinging jet, a short impingement distance is very efficient. On the other hand, many turbulent heat transfer phenomena of the impinging jet in a finite vessel which has both the impingement and side walls can be practically observed, where a round impingement jet is almost employed in. In this case, heat transfer rate on both impingement and side walls should be investigated to know heat efficiency in a whole finite vessel. In the practical engineering problems, a long impinging distance is observed in many cases. Thus, observations of heat transfer phenomena of impinging jet with long impinging distance should be also required, but the DNS is difficult to use for this problems due to the calculation cost. In this case, since a large eddy simulation (LES) and Reynolds averaged Navier-Stokes simulation (RANS) which might give the high accurate prediction are an efficiently technique for the observations, the prediction accuracy of LES or RANS should be evaluated using proper DNS or experimental data. Even out of these simulations, the LES can be expected to be able to observe the similar phenomena DNS obtained, but the proper turbulence model should be employed in the LES.

In this study, the DNS of turbulent heat transfer phenomena of round impinging jet in a finite vessel which is a circular container is conducted in order to observe and investigate characteristics of such heat transfer phenomena. Also, the LES of turbulent heat transfer phenomena of round impinging jet in a finite vessel is carried out, and the prediction of LES is evaluated using DNS data we obtained. DNS and LES are carried out under conditions of isothermal wall and various impinging distances to reveal an effect of impingement distance for an understanding of heat transfer phenomena, in which the detailed turbulent statistics, structures and mechanism of heat transfer are investigated.

DNS AND LES OF ROUND IMPINGING JET WITH HEAT TRANSFER

The governing equations of cylindrical coordinates system for the DNS of round impinging jet with heat transfer are the Navier-Stokes, the continuity and the energy equations which are assumed as incompressibility fluid as indicated below (Hattori *et al.*, 2015).

$$\frac{1}{r} \frac{\partial (ru_r)}{\partial r} + \frac{1}{r} \frac{\partial u_\phi}{\partial \phi} + \frac{\partial u_z}{\partial z} = 0 \quad (1)$$

$$\begin{aligned} & \frac{\partial u_r}{\partial t} + \frac{1}{r} \frac{\partial}{\partial r} (ru_r u_r) + \frac{1}{r} \frac{\partial}{\partial \phi} (u_\phi u_r) + \frac{\partial}{\partial z} (u_z u_r) - \frac{u_\phi^2}{r} \\ &= -\frac{\partial p}{\partial r} + \frac{1}{Re_D} \left[\frac{1}{r} \frac{\partial}{\partial r} \left(r \frac{\partial u_r}{\partial r} \right) - \frac{u_r}{r^2} + \frac{1}{r^2} \frac{\partial^2 u_r}{\partial \phi^2} + \frac{\partial^2 u_r}{\partial z^2} \right. \\ & \quad \left. - \frac{2}{r^2} \frac{\partial u_\phi}{\partial \phi} \right] \end{aligned} \quad (2)$$

$$\begin{aligned} & \frac{\partial u_\phi}{\partial t} + \frac{1}{r} \frac{\partial}{\partial r} (ru_r u_\phi) + \frac{1}{r} \frac{\partial}{\partial \phi} (u_\phi u_\phi) + \frac{\partial}{\partial z} (u_z u_\phi) + \frac{u_r u_\phi}{r} \\ &= -\frac{1}{r} \frac{\partial p}{\partial \phi} + \frac{1}{Re_D} \left[\frac{1}{r} \frac{\partial}{\partial r} \left(r \frac{\partial u_\phi}{\partial r} \right) - \frac{u_\phi}{r^2} + \frac{1}{r^2} \frac{\partial^2 u_\phi}{\partial \phi^2} \right. \\ & \quad \left. + \frac{\partial^2 u_\phi}{\partial z^2} + \frac{2}{r^2} \frac{\partial u_r}{\partial \phi} \right] \end{aligned} \quad (3)$$

$$\begin{aligned} & \frac{\partial u_z}{\partial t} + \frac{1}{r} \frac{\partial}{\partial r} (ru_r u_z) + \frac{1}{r} \frac{\partial}{\partial \phi} (u_\phi u_z) + \frac{\partial}{\partial z} (u_z u_z) \\ &= -\frac{\partial p}{\partial z} + \frac{1}{Re_D} \left[\frac{1}{r} \frac{\partial}{\partial r} \left(r \frac{\partial u_z}{\partial r} \right) + \frac{1}{r^2} \frac{\partial^2 u_z}{\partial \phi^2} + \frac{\partial^2 u_z}{\partial z^2} \right] \end{aligned} \quad (4)$$

$$\begin{aligned} & \frac{\partial \theta}{\partial t} + \frac{1}{r} \frac{\partial}{\partial r} (ru_r \theta) + \frac{1}{r} \frac{\partial}{\partial \phi} (u_\phi \theta) + \frac{\partial}{\partial z} (u_z \theta) \\ &= \frac{1}{Re_D Pr} \left[\frac{1}{r} \frac{\partial}{\partial r} \left(r \frac{\partial \theta}{\partial r} \right) + \frac{1}{r^2} \frac{\partial^2 \theta}{\partial \phi^2} + \frac{\partial^2 \theta}{\partial z^2} \right] \end{aligned} \quad (5)$$

On the other hand, the governing equations for LES are given as follows:

$$\frac{1}{r} \frac{\partial (r\bar{u}_r)}{\partial r} + \frac{1}{r} \frac{\partial \bar{u}_\phi}{\partial \phi} + \frac{\partial \bar{u}_z}{\partial z} = 0 \quad (6)$$

$$\begin{aligned} & \frac{\partial \bar{u}_r}{\partial t} + \frac{1}{r} \frac{\partial}{\partial r} (r\bar{u}_r \bar{u}_r) + \frac{1}{r} \frac{\partial}{\partial \phi} (\bar{u}_\phi \bar{u}_r) + \frac{\partial}{\partial z} (\bar{u}_z \bar{u}_r) - \frac{\bar{u}_\phi^2}{r} \\ &= -\frac{\partial \bar{p}}{\partial r} + \frac{1}{Re_D} \left[\frac{1}{r} \frac{\partial}{\partial r} \left(r \frac{\partial \bar{u}_r}{\partial r} \right) - \frac{\bar{u}_r}{r^2} + \frac{1}{r^2} \frac{\partial^2 \bar{u}_r}{\partial \phi^2} + \frac{\partial^2 \bar{u}_r}{\partial z^2} \right. \\ & \quad \left. - \frac{2}{r^2} \frac{\partial \bar{u}_\phi}{\partial \phi} \right] - \left[\frac{1}{r} \frac{\partial}{\partial r} (r\bar{u}_r \bar{u}_r - r\bar{u}_r \bar{u}_r) + \frac{1}{r} \frac{\partial}{\partial \phi} (\bar{u}_\phi \bar{u}_r - \bar{u}_\phi \bar{u}_r) \right. \\ & \quad \left. + \frac{\partial}{\partial z} (\bar{u}_z \bar{u}_r - \bar{u}_z \bar{u}_r) - \frac{1}{r} (\bar{u}_\phi \bar{u}_\phi - \bar{u}_\phi \bar{u}_\phi) \right] \end{aligned} \quad (7)$$

$$\begin{aligned} & \frac{\partial \bar{u}_\phi}{\partial t} + \frac{1}{r} \frac{\partial}{\partial r} (r \bar{u}_r \bar{u}_\phi) + \frac{1}{r} \frac{\partial}{\partial \phi} (\bar{u}_\phi \bar{u}_\phi) + \frac{\partial}{\partial z} (\bar{u}_z \bar{u}_\phi) + \frac{u_r u_\phi}{r} \\ &= -\frac{1}{r} \frac{\partial \bar{p}}{\partial \phi} + \frac{1}{Re_D} \left[\frac{1}{r} \frac{\partial}{\partial r} \left(r \frac{\partial \bar{u}_\phi}{\partial r} \right) - \frac{\bar{u}_\phi}{r^2} + \frac{1}{r^2} \frac{\partial^2 \bar{u}_\phi}{\partial \phi^2} \right. \\ & \quad \left. + \frac{\partial^2 \bar{u}_\phi}{\partial z^2} + \frac{2}{r^2} \frac{\partial \bar{u}_r}{\partial \phi} \right] - \left[\frac{1}{r} \frac{\partial}{\partial r} (r \bar{u}_r \bar{u}_\phi - r \bar{u}_r \bar{u}_\phi) \right. \\ & \quad \left. + \frac{1}{r} \frac{\partial}{\partial \phi} (\bar{u}_\phi \bar{u}_\phi - \bar{u}_\phi \bar{u}_\phi) + \frac{\partial}{\partial z} (\bar{u}_z \bar{u}_\phi - \bar{u}_z \bar{u}_\phi) \right. \\ & \quad \left. - \frac{1}{r} (\bar{u}_r \bar{u}_\phi - \bar{u}_r \bar{u}_\phi) \right] \end{aligned} \quad (8)$$

$$\begin{aligned} & \frac{\partial \bar{u}_z}{\partial t} + \frac{1}{r} \frac{\partial}{\partial r} (r \bar{u}_r \bar{u}_z) + \frac{1}{r} \frac{\partial}{\partial \phi} (\bar{u}_\phi \bar{u}_z) + \frac{\partial}{\partial z} (\bar{u}_z \bar{u}_z) \\ &= -\frac{\partial \bar{p}}{\partial z} + \frac{1}{Re_D} \left[\frac{1}{r} \frac{\partial}{\partial r} \left(r \frac{\partial \bar{u}_z}{\partial r} \right) + \frac{1}{r^2} \frac{\partial^2 \bar{u}_z}{\partial \phi^2} + \frac{\partial^2 \bar{u}_z}{\partial z^2} \right] \\ & \quad - \left[\frac{1}{r} \frac{\partial}{\partial r} (r \bar{u}_r \bar{u}_z - r \bar{u}_r \bar{u}_z) + \frac{1}{r} \frac{\partial}{\partial \phi} (\bar{u}_\phi \bar{u}_z - \bar{u}_\phi \bar{u}_z) \right. \\ & \quad \left. + \frac{\partial}{\partial z} (\bar{u}_z \bar{u}_z - \bar{u}_z \bar{u}_z) \right] \end{aligned} \quad (9)$$

$$\begin{aligned} & \frac{\partial \bar{\theta}}{\partial t} + \frac{1}{r} \frac{\partial}{\partial r} (r \bar{u}_r \bar{\theta}) + \frac{1}{r} \frac{\partial}{\partial \phi} (\bar{u}_\phi \bar{\theta}) + \frac{\partial}{\partial z} (\bar{u}_z \bar{\theta}) \\ &= \frac{1}{Re_D Pr} \left[\frac{1}{r} \frac{\partial}{\partial r} \left(r \frac{\partial \bar{\theta}}{\partial r} \right) + \frac{1}{r^2} \frac{\partial^2 \bar{\theta}}{\partial \phi^2} + \frac{\partial^2 \bar{\theta}}{\partial z^2} \right] \\ & \quad - \left[\frac{1}{r} \frac{\partial}{\partial r} (r \bar{u}_r \bar{\theta} - r \bar{u}_r \bar{\theta}) + \frac{1}{r} \frac{\partial}{\partial \phi} (\bar{u}_\phi \bar{\theta} - \bar{u}_\phi \bar{\theta}) \right. \\ & \quad \left. + \frac{\partial}{\partial z} (\bar{u}_z \bar{\theta} - \bar{u}_z \bar{\theta}) \right] \end{aligned} \quad (10)$$

where $\bar{(\)}$ means the filtered value for LES. The coordinates r , ϕ , z are the coordinate in the radial, circumferential and impingement wall-normal directions, respectively. Also, u_r , u_ϕ , u_z are the velocity components of each direction, respectively. Also, t is time, p is pressure, ν is the kinematic viscosity and α is the thermal diffusivity. In the DNS and LES, equations are nondimensionalized by the bulk velocity at the inlet, U_{zm} , the radius of inlet pipe, R ($= D/2$), where D is the diameter of inlet pipe, and temperature difference between the inlet and impingement wall temperature, $\Delta\Theta$ ($= \Theta_{in} - \Theta_w$). As for the calculation parameters appeared by the nondimensionalized equations, the Reynolds number based on the bulk velocity and the diameter of inlet pipe, Re_D ($= (U_{zm}D)/\nu$), is set as 4300, and the Prandtl number, Pr ($= \nu/\alpha$), is given as 0.71 assuming the air.

As for the turbulence models of LES which are required

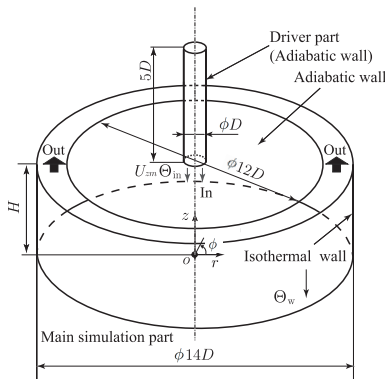


Figure 1. Computational domain, coordinate system and wall thermal conditions

to close the equations of Eqs. (6)~(10), the mixed time scale models for the eddy diffusivities in both the velocity and thermal fields (Inagaki *et al.*, 2005, 2012) are employed. The DNS and LES is carried out using the well-established high accuracy finite difference method with the cylindrical coordinate system (Hattori *et al.*, 2015, 2016), but the 6th-order accurate central difference is used for the spatial difference in ϕ direction in DNS and LES of this study. Also, the 3rd order low storage Runge-Kutta method is introduced for the time advancement of all terms except for molecular diffusion terms.

The configuration of calculation domain for a round impinging jet in a finite vessel is shown in Fig. 1, in which the fully-developing turbulent pipe flow with uniform temperature produced in the driver part is set as the inlet condition, i.e., the driver part gives turbulent jet. As for the outlet condition, a circular slit whose area is $13\pi D^2$ is arranged on the rim of upper wall as indicated in Fig. 1. Turbulent jet impinges the lower (impingement) wall, and then the fluid flow flows along the impingement wall and side wall, and a part of flow drains at the slit. Also, the impinging jet with turbulence yields heat transfer phenomena due to the isothermal wall condition on both the lower and side walls, where the upper wall is set as the adiabatic wall. The impingement distances are set $H/D = 2, 4$ and 8 . In the cylindrical coordinate system, since the grid resolution of radial direction becomes large toward downstream region on the impingement wall, the special attention is paid for the arrangement of grids (for instance, the grid resolutions of $r^+ \Delta\phi$ are $0.02 \sim 2.80$ in the DNS case of $H = 4D$, and the twice resolution is used for the LES). The grid points are arranged as 192 points for both the radial and circumferential directions in the DNS, and 96 points for both the radial and circumferential directions in the LES. The grid points for the impinging wall normal direction are arranged as 192 (case of $H/D = 2$), 384 ($H/D = 4$) and 768 ($H/D = 8$) for the DNS, and 96 (case of $H/D = 2$), 192 ($H/D = 4$) and 384 ($H/D = 8$) for the LES. The nondimensional time step, Δt , is 7.2×10^{-4} , and the DNS and LES are conducted until the well-developed turbulent statistics are obtained.

On the other hand, in order to preserve the energy balance in the calculation domain, the following relation should be maintained.

$$\begin{aligned} & E_{in} \cdot \pi R^2 + q_w \left[\pi (14R)^2 + 2\pi \cdot 14R \cdot H \right] \\ &= E_{out} \left[\pi (14R)^2 + \pi (12R)^2 \right] \end{aligned} \quad (11)$$

where, E_{in} ($= \rho c_p U_{zm} \Theta_{in}$) is the energy from the driver pipe, q_w ($= \lambda (\partial\theta/\partial z)|_{lower} - \lambda (\partial\theta/\partial r)|_{side}$) is the heat flux from both the lower and side walls, and E_{out} ($= \rho c_p U_{out} \Theta_{out}$) is

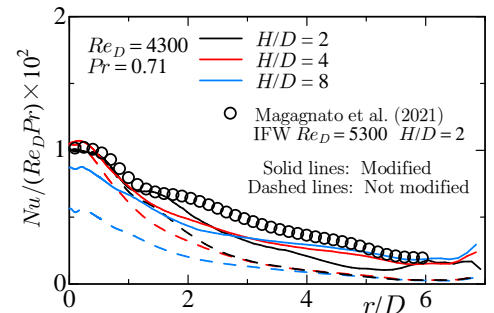


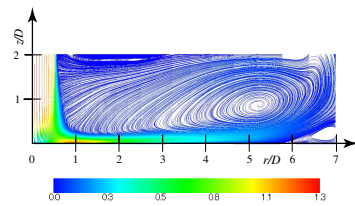
Figure 2. Distributions of modified local Nusselt numbers

the energy at the rim. Although this relation generally may be maintained by the boundary conditions, the inadequate results can be observed in the calculations. Thus, this relation is adopted so as to correct the energy balance in the calculations. Figure 2 shows the comparison between the results of local Nusselt number with correction and without correction. Obviously, the effect of correction can be observed, and the result is close to the other DNS result (Magagnato *et al.*, 2020) in the downstream region.

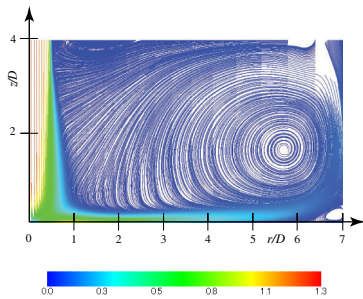
RESULTS AND DISCUSSION

Flow field structures

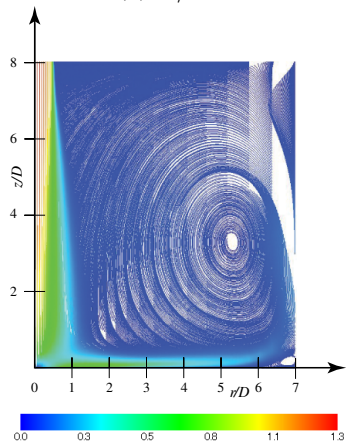
Figures 3 show the streamline of round turbulent impinging jet in the finite vessel obtained by DNS. In the turbulent jet blown from the inlet pipe, the potential core region can be seen in all cases, and then it is found the region vanished near the impinging wall due to the effect of wall in cases of $H/D = 2$ and 4. In the case of $H/D = 8$ as shown in Fig. 2(c), the potential core region of round jet is difficult to observe lower than $z/D = 4$, and then the velocity is decreased by both effects of development of round jet and the wall. It can be observed the flow impinges the wall, and then the flow redeveloped along the impingement wall. Moreover, appearance of



(a) $H/D = 2$



(b) $H/D = 4$



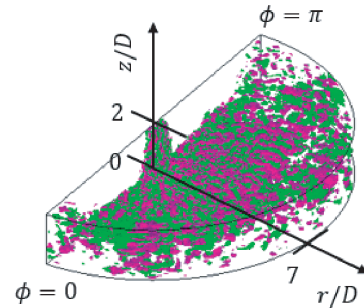
(c) $H/D = 8$

Figure 3. Streamline in round turbulent impinging jet with heat transfer by DNS

the large recirculation region in the downstream region due to existing the top and side walls and the separation region near the side wall are observed in all cases.

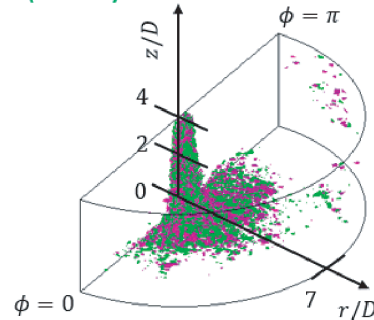
The vortex structures detected by the second invariant of gradients of velocity is indicated in Figs. 4. The vortex structures can be seen from the inlet, because the fully developed turbulent pipe flow blows from the inlet, and the structures are also found on the impinging wall. On the impinging wall, the vortex structures expand toward downstream region in all cases. In the case of $H/D = 2$ as shown in Fig. 3(a), the vortex structure can be seen on the side wall. In cases of $H/D = 4$ and 8, the vortex structures are not detected in the downstream region. This is because the laminarization of flow appears due to decrease of the flow rate of cross-sectional area which becomes large in the downstream region.

$\omega_r > 0$ (Purple)
 $\omega_r < 0$ (Green)



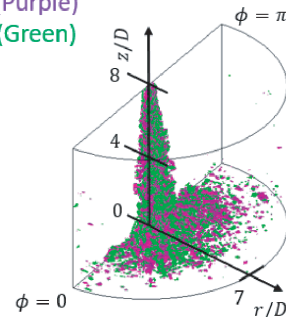
(a) $H/D = 2$

$\omega_r > 0$ (Purple)
 $\omega_r < 0$ (Green)



(b) $H/D = 4$

$\omega_r > 0$ (Purple)
 $\omega_r < 0$ (Green)



(c) $H/D = 8$

Figure 4. Vortex structure in round turbulent impinging jet with heat transfer by DNS

Fundamental turbulent statistics and evaluation of LES predictions

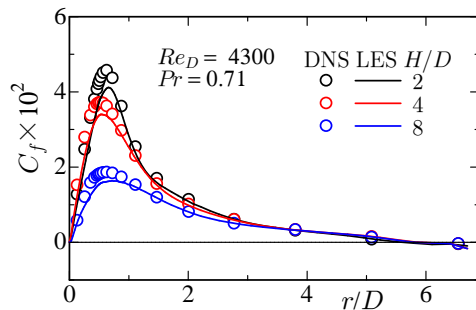
As a fundamental turbulent statistics, local wall friction coefficients and local Nusselt numbers along the impinging wall are indicated in Fig. 4. Note that results of LES are included in the following figures for the evaluation of LES predictions. The distributions of local friction coefficient obtained by DNS on the impinging wall indicate a rapid increase, and then take the peak value given away from the stagnation point in all cases. The peak values are obtained proportional to the impinging distance, in which the shortest impinging distance gives the largest peak value as shown in Fig. 4(a). From the point taking peak value, the friction coefficients of all cases slowly decrease toward downstream region, and finally these values become similar independently of impinging distance in the downstream region ($r/D > 5$). Also, near the side wall, the separation where the friction coefficient becomes negative value can be seen due to both the laminarization which is caused by becoming large cross section and the effect of

side wall. Thus, there is the influence of side wall near the side wall in this diameter of vessel, but the effect of side wall does not almost affect around the stagnation point.

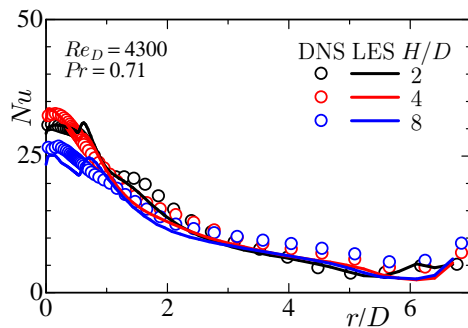
On the other hand, it is well-known that the stagnation point values of Nu are proportional to the impinging distance in general, but the stagnation point values of Nu are not so as shown in Fig. 5(b), in which the almost similar values of local Nusselt number in the cases of $H/D = 2$ and 4 are obtained. The reason why these local Nusselt numbers are obtained is discussed in the next section. In the downstream region from the stagnation point whose local Nusselt number takes the peak value, local Nusselt number slowly decreases on the impinging wall toward the side wall, and it can be also observed that the similar values of local Nusselt number in the all cases in the downstream region ($r/D > 5$). Near the side wall, the local Nusselt number of all cases slightly increases near the side wall due to both the separation and the influence of side wall whose thermal boundary condition is also a constant wall temperature.

The predicted local wall friction coefficients and local Nusselt numbers almost agree with the DNS results in all cases, but slight discrepancies of predicted Nusselt number can be observed near the point whose local friction coefficient takes the largest value in the region, i.e., overpredictions of local Nusselt number can be observed. Near the region, since the SGS eddy diffusivity for momentum becomes large, the SGS eddy diffusivity for momentum remarkably affects the SGS eddy diffusivity for heat. Thus, overpredictions of local Nusselt number are obtained. As for this prediction, the LES using the standard Smagorinsky SGS model (Smagorinsky, 1963) with the wall damping and a constant SGS Prandtl number function is also carried out, but the similar results are obtained.

In order to observe the heat transfer performance, the ratio of wall friction coefficient and j -factor which is defined by $j_H = Nu/(Re_D Pr^{1/3})$, which indicates the efficient of heat transfer and the similarity between the velocity and thermal fields as shown in Fig.6. Since the ratios are over unity between $r/D = 1$ and 3, the influence of friction force of flow is greater than that of heat transfer in this region. And, near the stagnation point and side wall, the values in all cases take under unity, so the efficient of heat transfer is larger than the friction force, i.e., the heat transfer performance is well. Near the stagnation point, the reason why the heat transfer performance is well the thermal boundary layer faster develops than velocity boundary layer. In the downstream region near the side wall, it can be considered that the heat transfer performance is well due to the laminarization and separation. Also, from this result, the values of ratio obviously indicate the dissimilarity between velocity and thermal fields in all cases.



(a) Local wall friction coefficients



(b) Local Nusselt numbers

Figure 5. Distributions and comparisons of LES predictions with DNS: Fundamental parameters

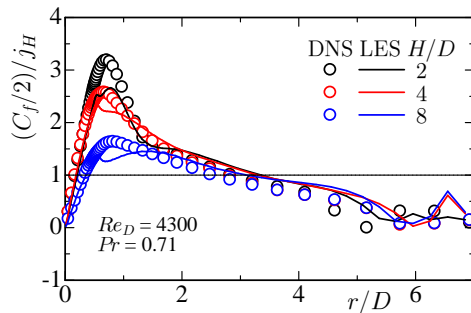
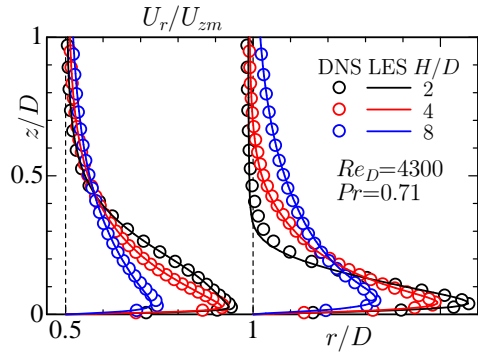


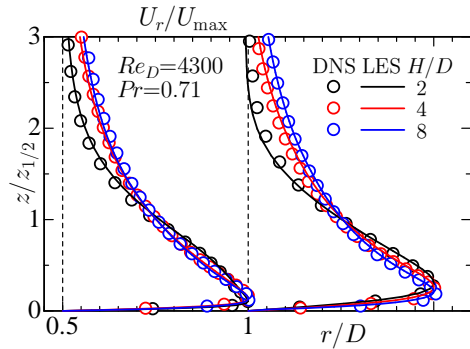
Figure 6. Distributions and comparisons of LES predictions with DNS: Ratio of wall friction coefficient and j -factor

Distributions of turbulent quantities and evaluation of LES predictions

The distributions of radial wise mean velocities near the stagnation point and the wall are shown in Fig. 7, in which the predictions of LES are included for the evaluation. Since the radial wise mean velocity develops as the wall jet along the impinging wall, two normalizations are adopted. Figure 7(a) shows the radial wise mean velocities normalized by the characteristic velocity, U_{zm} , and the mean velocities normalized by both the maximum value of local mean velocity, U_{max} and the half-value width of the wall jet in the free shear region, $z_{1/2}$. The profiles of radial wise mean velocity obviously indicate similar profile without regard to the impingement distance as shown in Fig. 7(b), though the different profiles are shown in

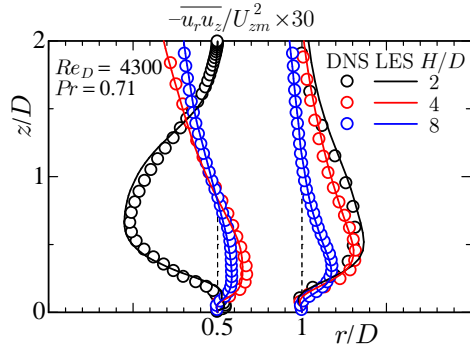


(a) Normalized by the characteristic velocity

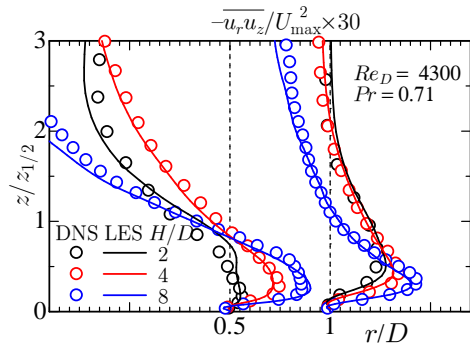


(b) Normalized by the local mean velocity at the half value of width

Figure 7. Distributions and comparisons of LES predictions with DNS: Radial wise mean velocity



(a) Normalized by the characteristic velocity

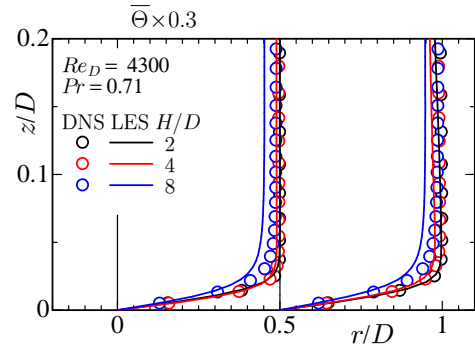


(b) Normalized by the local mean velocity at the half value of width

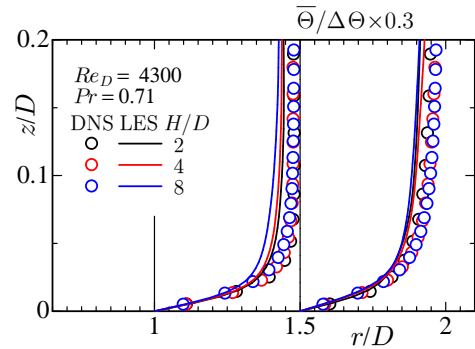
Figure 8. Distributions and comparisons of LES predictions with DNS: Reynolds shear stresses

Fig 7(a) . As for the LES predictions, it can be found that the radial wise mean velocity are properly predicted by the LES.

Figures 8 indicate the distributions of Reynolds shear

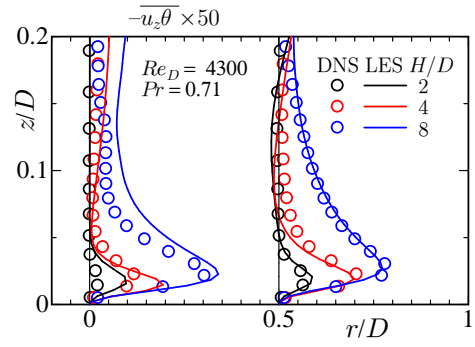


(a) $r/D = 0 \sim r/D = 0.5$

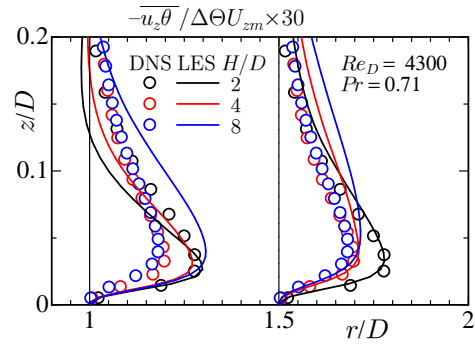


(b) $r/D = 1.0 \sim r/D = 1.5$

Figure 9. Distributions and comparisons of LES predictions with DNS: Mean temperature



(a) $r/D = 0 \sim r/D = 0.5$



(b) $r/D = 1.0 \sim r/D = 1.5$

Figure 10. Distributions and comparisons of LES predictions with DNS: Wall-normal turbulent heat fluxes

stresses in wall-normal direction with z/D and $z_{1/2}$, in which the predictions of Reynolds shear stress by LES are also included in these figures, and it can be seen that the predictions are in good agreement with DNS results. In Fig. 8(a), the profile of Reynolds shear stress in the case of $H/D = 2$ can be differently seen in comparison with other cases, but the similar profiles can be found in Fig. 8(b). Thus, adopting the half-value width of the wall jet in the free shear region, $z_{1/2}$, the near-wall distribution of Reynolds shear stress can be similarly demonstrated with the different impinging distance. The profiles, however, do not indicate similar profile as like the profiles of radial wise mean velocity, because the points of near-wall maximum values of Reynolds shear stress in each case disagree. This discrepancies of Reynolds shear stress distributions give the different peak values of local wall friction coefficient. Also, it can be found in the normalization using $z_{1/2}$ that the points which are the zero radial wise mean velocity gradient disagree with the points which are zero of Reynolds shear stress.

Regarding the thermal field, the profile of mean temperature distribution forms as a boundary layer, so the normalization of wall-normal distance using $z_{1/2}$ may not be adopted. Thus, distributions of mean temperature from the stagnation point with the wall-normal distance, z/D , are shown in Fig. 9, in which the LES predictions are also included. It can be found that the LES predictions give disagreement results in comparison with DNS results. As for the DNS results, it can be observed that the temperature gradient near the wall becomes small in all cases toward the downstream region, which is consistent with the distributions of local Nusselt number. This is because the local Nusselt number only depends on the temperature gradient due to a constant temperature condition on the impinging wall.

Figure 10 shows the distributions of wall-normal turbulent heat flux including the LES predictions. At the stagnation point, the wall-normal turbulent heat flux of LES predictions in the cases of $H/D = 2$ and 4 gives overpredictions near the wall in comparison with DNS results. Since the temperature gradients of these cases almost agree with the DNS result, it can be seen that these overpredictions are difficult to affect the predicted profiles of mean temperature. In view of DNS result, the wall-normal turbulent heat flux does not influence the temperature profile in the case of $H/D = 2$, but the wall-normal turbulent heat flux slightly affects the temperature profile in the case of $H/D = 4$. Thus, obtaining the similar values of local Nusselt number at the stagnation point in the cases of $H/D = 2$ and 4 as indicated in Fig. 5(b) is due to the difference effect of wall-normal turbulent heat flux, i.e., turbulence does not affect at the stagnation point in the case of $H/D = 2$. Returning the evaluation of LES prediction, observing the rapid increases of local Nusselt number in all cases around the point taking maximum value of friction coefficient as shown in Fig. 5(b) is due to discrepancies of wall-normal turbulent heat flux between LES predictions and DNS results as indicated in Fig. 10(b). As for the this reason, the effect of SGS eddy diffusivities remarkably influence as mentioned forgoing section, so it may be necessary to pay attention when an LES of round impinging jet with heat transfer using Smagorinsky SGS type turbulence model is carried out.

CONCLUSIONS

The DNS and LES of turbulent heat transfer phenomena of round impinging jet in a finite vessel with various impinging distances are successfully carried out in order to evaluate

an LES prediction and to observe the heat transfer phenomena in a finite vessel. The predictions of LES are evaluated using DNS data, as the result, it is assessed that the LES can qualitatively predict such phenomena. In the results of DNS, the effect of impingement distance for the heat transfer on the impinging wall can be clearly found, but similar local Nusselt numbers at the stagnation point are obtained in both the cases of $H/D = 2$ and $H/D = 4$. Concerning the reason for obtaining similar values, it is found that the distributions of temperature and the impinging wall normal turbulent heat flux near the wall are related, in which the wall normal turbulent heat flux remarkably affects in the case of $H/D = 4$. Also, the streamline and vortex structure are obviously indicated to show the characteristics of flow situation in the finite vessel. In the downstream region on the impinging wall, since the laminarization appears due to becoming large cross section and there is the side wall, it can be seen that the flow separation occurs in all cases. The effect of side wall, however, only influences near the side wall, but the effect can not be seen around the stagnation point in this diameter of vessel. As for the efficiency of heat transfer, the wall frictions in all cases are greater than heat transfer rate around the point taking the maximum value of friction coefficient. Thus, it is found that the effective heat transfer rate is mainly obtained around stagnation point. Therefore, DNS and LES reveals the characteristics, structures, and statistical quantities of turbulent heat transfer of a round impinging jet with various impinging distances in a finite vessel.

ACKNOWLEDGEMENTS

This work is the result of a collaborative research program with the Research association of Automotive Internal Combustion Engines (AICE) for fiscal years 2020-2021.

REFERENCES

- Hattori, H., Hosyaku, A., Kamiya, K., Houra, T. & Tagawa, M. 2015 Dns for turbulent heat transfer in thermal entrance region of pipe flow. *Proceedings of the Asian Symposium on Computational Heat Transfer and Fluid Flow -ASCHT2015* p. 6 pages in USB.
- Hattori, H., Inagaki, M., Houra, T. & Tagawa, M. 2016 Direct numerical simulation of thermal entrance region in combined turbulent pipe flow. *Proceedings of the 11th International ERCOFTAC Symposium on Engineering Turbulence Modelling and Measurements -ETMM11-* p. 6 pages.
- Hattori, H. & Nagano, Y. 2004 Direct Numerical Simulation of Turbulent Heat Transfer in Plane Impinging Jet. *International Journal of Heat and Fluid Flow* **25**, 749–758.
- Inagaki, M., Hattori, H. & Nagano, Y. 2012 A mixed-timescale SGS model for thermal field at various Prandtl numbers. *International Journal of Heat and Fluid Flow* **34**, 47–61.
- Inagaki, M., Kondoh, T. & Nagano, Y. 2005 A mixed-timescale sgs model with fixed model-parameters for practical LES. *Journal of Fluids Engineering* **127**, Issue 1, 1–13.
- Magagnato, F., Secchi, F., Foroughi, P., Straub, S. & Frohnafel, B. 2020 Dns of turbulent heat transfer in impinging jets at different Reynolds and Prandtl numbers. *Proceedings of 14th WCCM-ECCOMAS Congress 2020* p. 12 pages.
- Smagorinsky, J 1963 General circulation experiments with the primitive equations. *Monthly Weather Review* **91**, 99–164.